Hindawi
Mathematical Problems in Engineering
Volume 2022, Article ID 6204795, 13 pages
https://doi.org/10.1155/2022/6204795

Research Article

Research on Optimization of Structural Parameters of Equipment Cabin Bottom Cover

Hua Zou,[1] **Qifeng Wu**,[1] **and Yonggui Zhang**[2]

[1]*School of Mechanical, Electric and Control Engineering, Beijing Jiaotong University, Beijing 100044, China*
[2]*CRRC Qingdao Sifang Co., Ltd., Qingdao 266111, China*

Correspondence should be addressed to Hua Zou; hzoubjtu@126.com

Received 23 June 2022; Revised 22 July 2022; Accepted 1 August 2022; Published 22 August 2022

Academic Editor: Wei Liu

Since the railway vehicle structure has lots of parameters and several complex constraints, this study establishes a method for structural parameter optimization based on sensitivity analysis and surrogate models. Fatigue crack problem of the equipment cabin bottom cover of the EMU is taken as an example to optimize its structural parameters. First, establish the finite element (FE) model of the bottom cover and compare it with the bench test results to verify the accuracy of the load and restraint conditions. The sensitivity analysis method is used to determine the main parameters. The input samples are obtained by Latin hypercube sampling method, and the output samples are obtained by the method jointly developed by ABAQUS+Python and the surrogate model between the input and output samples is obtained by fitting, and its accuracy is verified. According to the design requirements, the optimization objective function and constraint conditions are established, and the optimization result is obtained by optimization algorithm. The results were substituted into the FE model for verification. The results show that the maximum equivalent stress of the bottom cover is reduced from 126.7 MPa to 78.9 MPa under a cyclic aerodynamic load of ±4 kPa, which is 37.7% optimized, and the effect is significant. This method avoids the iterative optimization of the FE model and improves the optimization efficiency.

1. Introduction

In the application of large mechanical structural parts, fatigue cracks have always been the main factor leading to their failure [1–3]. Take railway vehicles as an example; fatigue cracks are found on the equipment cabin bottom cover. The reason is that the alternating aerodynamic load under the working conditions when trains enter and exit tunnels is the main factor leading to the initiation and propagation of cracks [4]. Therefore, it is necessary to study the structural optimization design method to reduce the stress level at the crack under alternating aerodynamic loads.

Nowadays, there has been in-depth research on the optimization method of structural parts [5]. The authors in [6–11] separately optimized the structure of energy-absorbing structure, carbody structure, and the subway vehicle air-conditioning suspension. Their weights were reduced while meeting the requirements of strength and modal. But for the bottom cover, its protection function and manufacturability need to be considered, so the topology optimization results often do not have engineering application value. The authors in [12, 13] optimized the shape of the frame and wheel. But the shape optimization required modification of the floor structure. At the same time, it was also necessary to consider constraints such as installation, connection, and manufacturability, so the space for modification was limited. The size optimization does not require major changes to the floor structure, which is relatively easy to implement and has high engineering value. Therefore, this article uses the size optimization method to optimize the bottom cover.

Now scholars have begun to use a variety of methods to optimize the parameters of the structure [14–16]. Among them, approximate methods have been widely used [17]. For the railway vehicle structure, the structure is complex and the boundary conditions are numerous, which often requires a lot

of time in the simulation calculation. In order to improve the optimization efficiency, many scholars have conducted research on the optimization method of size parameters. Myzrglob and Zielinski [18, 19] studied the optimization method of structural parameters under multi-axial high-cycle fatigue. Sun et al. and Hudson et al. [20, 21] studied the optimization method of carbody parameters considering multiple factors. Sun et al. [22] optimized the modal frequency of the railway vehicle carbody based on SA. Miao et al. [23] used the ant colony algorithm to optimize the composite sandwich structure of the bottom cover. Zhi et al. [24] studied the fuzzy optimization method of bogie frame parameters based on response surface model. Baek et al. [25] optimized the wagon frame structure based on the Chebyshev polynomial model. The authors in [26–28] used surrogate models and multi-objective genetic algorithms to optimize the design of the carbody collision energy absorption structure. The authors in [29–31] optimized the fatigue strength of the welded frame weld by the surrogate model method.

The above research used mathematical models to express the relationship between structural parameters of vehicle components such as carbody, bogie frame, and energy-absorbing structure with modal and strength indicators and optimized them with optimization algorithms to improve optimization efficiency. However, the optimization research on the equipment cabin bottom cover is still lacking at the present stage, and the connection and contact between the various components cannot be ignored for this type of assembly. There are many size parameters and installation parameters of components, and each parameter has a complex nonlinear relationship with the stress response of key points. Establishing a FE model that can reflect the actual components and meet the requirements of optimization accuracy is a prerequisite for optimization design. For this reason, this paper carried out the static strength test of the bottom cover and compared the FE calculation results with the test results to verify the accuracy of the FE model. Considering the complex preprocessing of the FE model and the long calculation time, this paper first extracts the key parameters of the bottom plate according to the sensitivity analysis (SA) method and uses the optimal Latin hypercube sampling to obtain the input sample set of the key parameters. Through the ABAQUS + Python cosimulation method, the FE model under different input parameters is obtained in batches, and the output parameter samples are obtained. Then, the surrogate model is fitted to replace the FE model, and optimization is performed based on the optimization algorithm. This method can effectively improve optimization efficiency.

2. Structural Parameter Optimization Design Method

2.1. Parameter Optimization Process Based on FE Model. In the FE model, due to the model scale, contact nonlinearity, material nonlinearity, and other issues, it often takes a long time to simulate. At the same time, optimization research needs to modify the parameters multiple times for iterative calculations, so there are many repeated calculations. If the FE model is directly called, it will consume a lot of time and be inefficient. Therefore, in order to improve the optimization efficiency under the premise of ensuring accuracy, the optimization method shown in Figure 1 can be used for the complicated FE model.

According to Figure 1, firstly, the SA method is used to screen the optimized parameters, and then the optimal Latin hypercube sampling or orthogonal test is used to sample in the range to obtain a uniform and representative parameter sample set. Use the Python program to read the samples in order, modify the parameters of the FE model in ABAQUS, submit calculations, and read the stresses at the key points. Summarize the stress values under different samples and use them as input and output parameters. Use the above input and output parameters as samples and import them into the Isight software to fit the surrogate model and evaluate the goodness of fit. Based on the surrogate model, optimization algorithms such as steepest descent method and genetic algorithm are used for optimization. Then, the optimal solution of the model is obtained and imported into ABAQUS for verification.

2.2. Parameter SA Method. When there are many optimization parameters, the amount of calculation in sampling calculation and optimization calculation is large. The parameter SA method can eliminate the parameters that have little influence on the result. Assuming that there are n parameters, there is the following functional relationship between the i-th parameter p_i and the response r:

$$r = r(p_1, p_2, p_3, \ldots, p_n). \tag{1}$$

The sensitivity ε_i of different parameters can be expressed by the following formula:

$$\varepsilon_i = \frac{\partial r(p_1, p_2, p_3, \ldots, p_n)}{\partial p_i}, \quad i = 1, 2, 3, \ldots, n. \tag{2}$$

It is often a discrete variable in engineering applications. Its sensitivity ε_i can be expressed by the finite difference method:

$$\varepsilon_i = \frac{r(p_i + \Delta p_i) - r(p_i)}{\Delta p_i}, \quad i = 1, 2, 3, \ldots, n. \tag{3}$$

However, when calculating the sensitivity through the above formula, the influence of the parameter scale and the variation range is ignored. When the parameter scale is large, the calculated sensitivity is often small. Therefore, the original parameter value p_{i0} and the original response value r_0 are used as scale factors, and the sensitivity parameters are normalized:

$$\varepsilon_i = \frac{[r(p_i + \Delta p_i) - r(p_i)]/r_0}{\Delta p_i / p_{i0}}, \quad i = 1, 2, 3, \ldots, n. \tag{4}$$

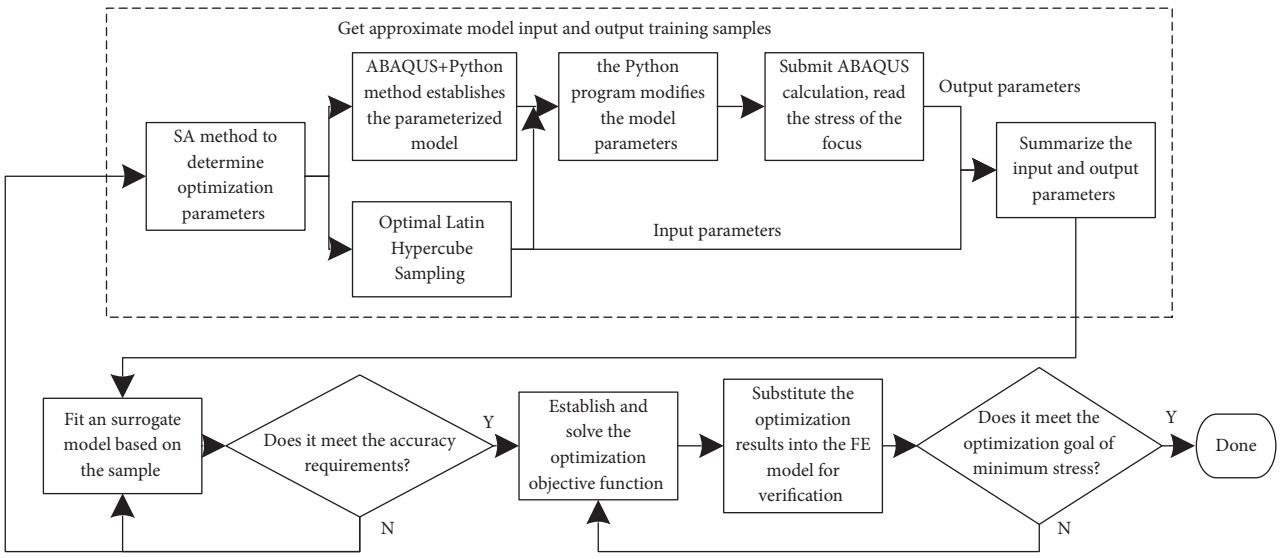

Figure 1: Bottom cover optimization method.

In order to improve the accuracy of the sensitivity parameter, take m different difference step size Δp_{ij} ($j = 1, 2, 3, \ldots, m$, including the original value, $\Delta p_{i1} = 0$) within the parameter change range. The least square method is used to fit it into a proportional function relationship of $r_i = k_i p_i$, and the absolute value of the slope k_i is taken as the sensitivity parameter:

$$\varepsilon_i = \left|k_i\right| = \left|\frac{\sum_{j=1}^{m} R_{ij} P_{ij}}{\sum_{j=1}^{m} R_{ij}^2}\right|, \quad i = 1, 2, 3, \ldots, n, \quad j = 1, 2, 3, \ldots, m, \tag{5}$$

where

$$R_{ij} = \frac{\left[r\left(p_i + \Delta p_{ij}\right) - r\left(p_i\right)\right]}{r_0}, \qquad P_{ij} = \frac{\Delta p_{ij}}{p_{i0}}. \tag{6}$$

2.3. Sample Acquisition Method Based on FE Model. According to the optimized parameters and their ranges, a set of representative input parameters needs to be extracted. The optimal Latin hypercube sampling method has strong filling ability, uniform sample distribution, and good representativeness. Assuming that a total of m samples are required, m small hypercubes are randomly selected in the n-dimensional hypercube space composed of n design variables to ensure that each small hypercube is unique in each design variable interval. That is, each design variable will be sampled only once at each level. In this way, a Latin hypercube design matrix with m samples under n design variables is obtained. At the same time, through the optimization algorithm, the Euclidean distance between different sample points is minimized, and the evenly distributed and representative sampling results are obtained. This paper uses the optimal Latin hypercube method to sample the parameters. Generate the optimal Latin hypercube sampling results in Isight software as input samples.

The FE model is established based on the input parameters, and the output parameters can be obtained through FE simulation. ABAQUS has a powerful secondary development function. Using Python programs, it can perform secondary development on the preprocessing and postprocessing parts of ABAQUS, achieve automatic modeling, automatic submission calculations, and automatic postprocessing batch calculations, which can save simulation time.

Figure 2 shows the parameter flow of using the Python program to obtain the output. First read a set of input parameters from the input parameter set and import the ABAQUS library function into the program, and the ABAQUS library function contains members that can be used for modeling. The members in the Model object under the Mdb object can be used for preprocessing work such as building 3D models, defining material properties, meshing, and defining loads and constraints. The Job object can submit calculations to the model. Each member under the Odb object can read the field output and history output results in the calculated odb result file to obtain the required output parameters. In this loop, the output parameters under different input parameters can be obtained, and the output parameter set can be summarized. The input parameter set and the output parameter set are combined as surrogate model training samples.

2.4. Surrogate Model Establishment Method. Isight software provides a variety of surrogate model fitting algorithms, including response surface model (RSM), radial basis function neural network (RBFNN) model, Kriging model, and so on.

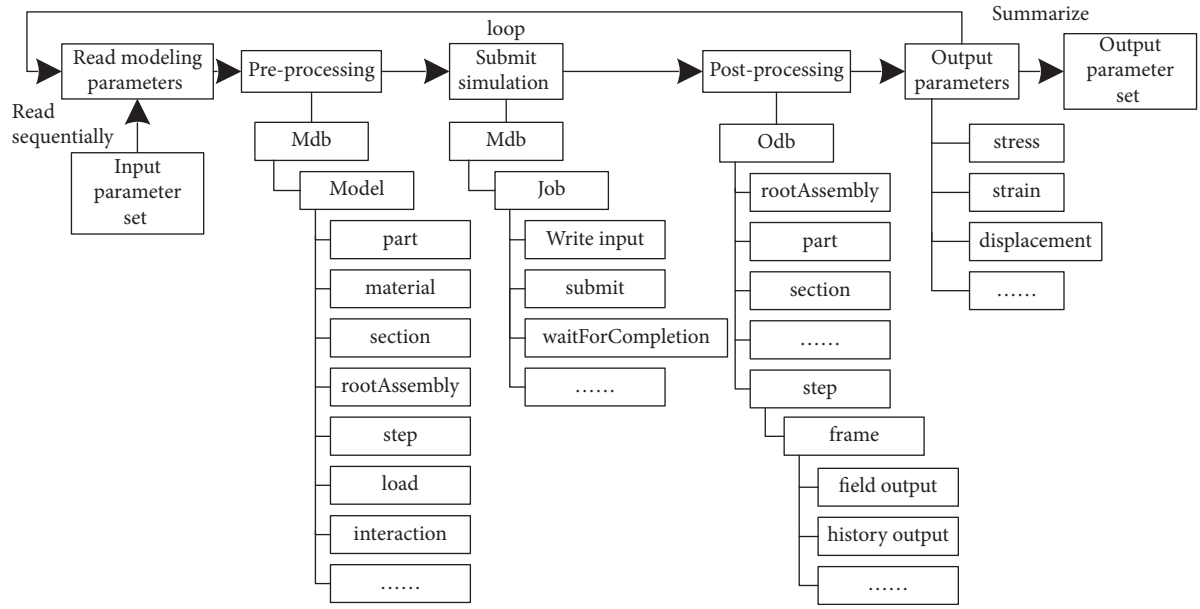

Figure 2: Sample acquisition process based on FE parameter model.

2.4.1. Response Surface Model (RSM). Taking the fourth-order response surface model as an example, the surrogate model fitting formula is shown in the following equation:

$$\begin{aligned}\hat{y} = \beta_0 + \sum_{i=1}^{M} \beta_i x_i + \sum_{i=1}^{M} \beta_{M+i} x_i^2 + \sum_{i=1}^{M} \beta_{2M+i} x_i^3 \\ + \sum_{i=1}^{M} \beta_{3M+i} x_i^4 + \sum_{i \neq j} \beta_{ij} x_i x_j,\end{aligned} \tag{7}$$

where M is the number of input variables; x_i represents the input variables; $\hat{y}$ is the output value; and β_i represents the coefficients.

2.4.2. Kriging Model. The expression of the Kriging model is shown in the following equation:

$$\hat{y} = f^T(x)\beta + Z(x), \tag{8}$$

where $f^T(x)\beta$ is the global regression model; $Z(x)$ is the random fluctuation; and $\hat{y}$ is the output value.

2.4.3. Radial Basis Function Neural Network (RBFNN) Model. In the RBFNN model, the radial function is the basis function of the model, and its independent variable is the Euclidean distance between the measured point and the input point. (3) is the basic form of the radial basis function.

$$\hat{y} = \sum_{j=1}^{M} H_j(r) w_j = \mathbf{H}^{\mathbf{T}}(r)\mathbf{w}, \tag{9}$$

where w_j is the weight; M is the number of samples; $H_j(r)$ is the radial function; and $\hat{y}$ is the output value. By adjusting the weights, the radial basis function can be used to fit different models.

There are many indicators for evaluating the goodness of fit of a surrogate model. The normalized root mean square error (NRMS) and certainty coefficient (R2) are commonly used to evaluate the global goodness of fit [32]. The expression of the NRMS is

$$\text{NRMS} = \sqrt{\frac{\sum_{i=1}^{N} (y_i - \hat{y}_i)^2}{\sum_{i=1}^{N} y_i^2}}. \tag{10}$$

The value range of NRMS is [0, 1]. The closer its value is to 0, the better the goodness of fit is. Its threshold value is 0.1.

The expression of R^2 is

$$R^2 = 1 - \frac{\sum_{i=1}^{n} (y_i - \hat{y}_i)^2}{\sum_{i=1}^{n} (y_i - \overline{y})^2}. \tag{11}$$

The value range of R^2 is [0, 1]. The closer its value is to 1, the better the goodness of fit is. Its threshold value is 0.9.

y_i is the sample value, $\overline{y}$ is the sample mean, and $\hat{y}_i$ is the surrogate model predicted value.

2.5. Optimization Method. The optimization problem with constraints can be expressed as

$$\min_x f(x), x \in \mathbf{R}^{\mathbf{n}}, \tag{12}$$

$$s.t. \begin{cases} g_i(x) \leq 0, \\ h_i(x) = 0. \end{cases} \tag{13}$$

(12) is the optimization objective function. (13) is the optimization constraint, where $g_i(x)$ is an inequality constraint and $h_i(x)$ is an equality constraint. When solving the above two equations, in order to obtain reliable optimization results, it is often necessary to resort to optimization algorithms. Optimization algorithms can be divided into

numerical and exploratory types. Among them, the numerical optimization algorithm has a faster calculation speed and fewer iterations, but it is easy to fall into a local minimum. Representative algorithms include NLPQLP (continuous quadratic programming method), LSGRG (generalized gradient descent method), and so on. Exploratory optimization technology can search the whole world and is not easy to fall into the local minimum, but there are relatively many iterations. Among them, the representative algorithm is genetic algorithm, and the process is shown in Figure 3. Commonly used genetic algorithms include MIGA (multi-island genetic algorithm), NSGA-II (nondominant sorting genetic algorithm), and so on.

3. Establishment and Verification of the Equipment Cabin Bottom Cover FE Model

The equipment cabin bottom cover structure is shown in Figure 4. The main body is a flat plate, which is reinforced by three rectangular tube beams. The plate size is 1144×576 mm. The flat plate and rectangular tube beams are formed by bending 2 mm thick cold-rolled SUS304 stainless steel plates. The bottom cabin is fixed to the side beam of the equipment cabin by a total of eight bolts and backing plates at both ends.

3.1. Static Strength Test of Bottom Cover. The static strength test of the equipment cabin bottom cover is carried out under the conditions of the indoor fatigue test bench, and the stress measurement points are arranged at the key positions of the bottom cover as shown in Figure 5. Vacuum suction cups are uniformly arranged on the surface of the bottom cover to simulate the aerodynamic uniform load. The MTS fatigue testing machine is used to load the aerodynamic load under tension and compression at 4 kPa. The static strength test method and tooling under aerodynamic load are as described in the literature [33]. After the loading force is stable, use TDS-530 static data acquisition instrument to collect strain data. The loading tooling is shown in Figure 6.

3.2. Bottom Cover FE Model. Based on the 3D model of the bottom cover, the FE model of the bottom cover is established in ABAQUS. The flat plate and rectangular tube beam of the bottom cover are extracted from the midsurface and divided into shell elements. Divide the backing plate into solid elements. Both ends simplify the equipment cabin bracket to a discrete rigid body, imitating the fixing of the equipment cabin bracket to the bottom cover. The FE model is shown in Figure 7.

The position of the rivet hole between the flat plate, rectangular tube beam, and backing plate adopts beam element and rigid element to imitate riveting, and the contact pairs are set between each surface as shown in Table 1. A fixed constraint is applied to the equipment cabin bracket and backing plate bolts, and a uniformly distributed aerodynamic load of ±4 kPa is applied to the surface of the bottom cover. Simulations show that the model can converge reliably.

3.3. Validation of the FE Model. The measurement points with relatively large stress values and relatively small stress gradients are selected to prevent the effect of stress concentration and the zero point error of the strain gauge from affecting the results. The results are compared with the output results of the FE model to verify the FE model. The comparison between the FE simulation results and the test results of some measuring points is shown in Table 2:

In Table 2, measuring points 2, 3, and 4 are the corner positions of the edge of the flat plate, and measurement points 12 to 17 are the process hole edges of the middle rectangular tube beam. In comparison, with the exception of the relatively large gap between measurement point 13 and measurement point 16, the measured stresses of the remaining measuring points are relatively close to the simulated stresses, indicating that the boundary condition settings of the FE model are basically consistent with the actual model. Measuring point 13 and the measuring point 16 are located at the edge of the center process hole rectangular tube beam, where the stress gradient is relatively large due to the stress concentration effect. Therefore, the attachment position of the strain gauge has a greater influence on the final result. The test result is different from the result of the FE model, but the trend is the same, which does not affect the direction and accuracy of the optimization.

Through FE analysis, under aerodynamic loads of ±4 kPa, the maximum normal stress of the bottom plate appears on the edge of the center process hole rectangular tube beam (its location is marked by the box in Figure 8), and the direction is along the length of the rectangular tube beam. The stress distribution at the edge of the process hole and the maximum nodal stress value are shown in Figure 8.

Under pull working conditions, the maximum nodal stress is −130.7 MPa, and the maximum integration point stress is −138.2 MPa read by Python program; under push working conditions, the maximum nodal stress is 114.1 MPa, and the maximum integration point stress is 119.6 MPa. The nodal stress is obtained by extrapolating the integration point stress. In the following optimization calculations, the integration point stress is used.

In summary, the FE model can imitate the actual model well, and it can converge reliably, ensuring the accuracy of the optimization.

3.4. Calculation of Equivalent Stress under Symmetrical Cycle. Due to the influence of factors such as contact nonlinearity, when the bottom cover is subjected to a symmetrical cycle of pull and push load, its stress response is not necessarily a symmetrical cycle. The FE method is used to obtain the stress peak-valley value, average stress, and stress amplitude of the bottom cover under ±4 kPa aerodynamic load. The equivalent stress σ_{-1} under symmetrical cycles can be calculated by the Goodman equation (hereinafter referred to as equivalent stress):

$$\sigma_{-1} = \frac{\sigma_a}{1 - \sigma_m/\sigma_u}, \tag{14}$$

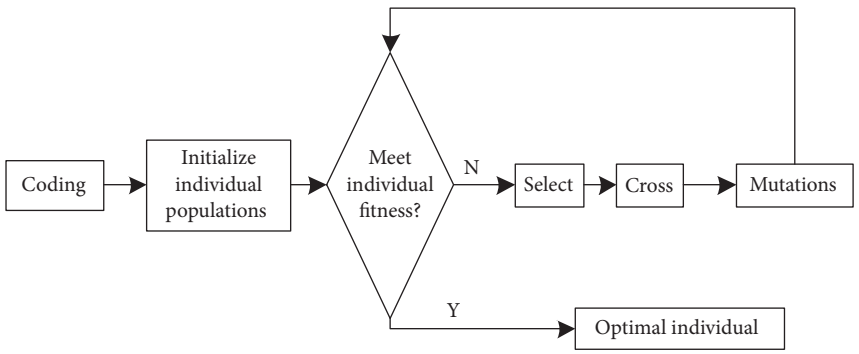

Figure 3: The basic process of genetic algorithm.

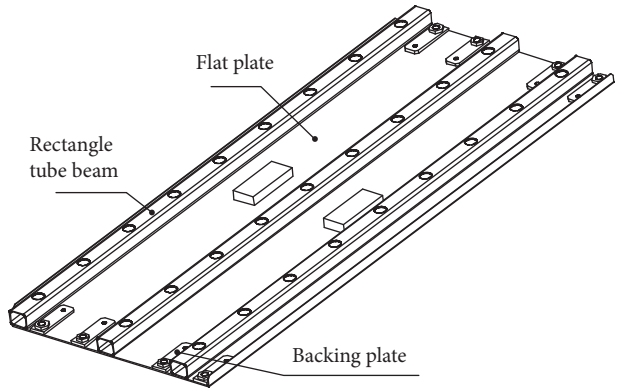

Figure 4: Structure of bottom cover.

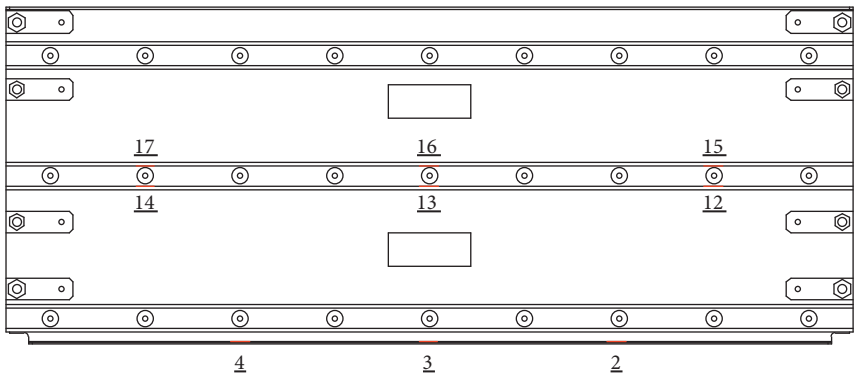

Figure 5: Bottom cover measurement point layout.

where σ_a is the stress amplitude, σ_m is the average stress, and σ_u is the ultimate strength of the material. Tensile test is performed on the small sample of the bottom plate on the MTS-810 universal material testing machine, and the mechanical properties are shown in Table 3.

In ABAQUS, the integration point stress of each element under pull and push conditions can be read through the Python program. Then, the equivalent stress of each element at the integration point can be calculated by (14).

4. Structural Parameter Optimization Design of Equipment Cabin Bottom Cover

4.1. Parameter Selection and SA. Combined with the survey results, cracks mostly appeared in the weak points of the hole edge of the rectangular tube beam. After FE analysis and static strength bench test, the edge of the center process hole rectangular tube beam (measurement points 13 and 16 in Figure 5) has relatively high stress, which is likely to be the initiation of cracks. Taking into account factors such as

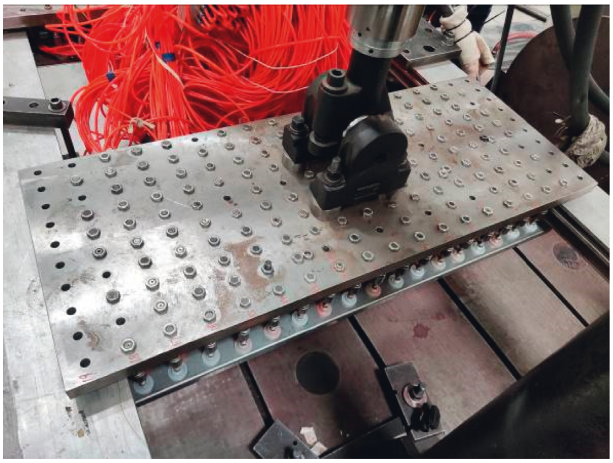

Figure 6: Bottom cover loading tool.

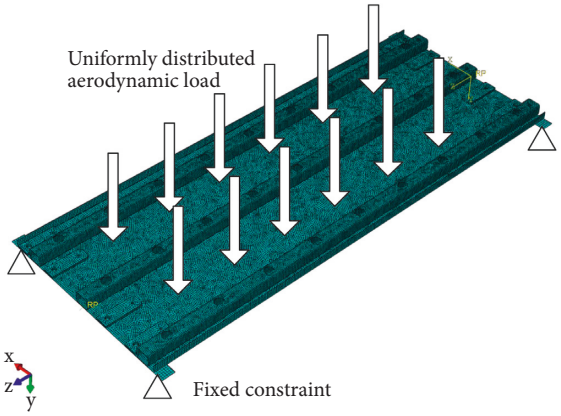

Figure 7: FE model of bottom cover.

Table 1: Contact attribute settings for each contact pair.

No.	Master surface	Slave surface	Discretization method	Contact property options
1	Flat plate lower surface	Rectangular tube beam upper surface	Surface to surface	Hard contact friction coefficient: 0.15
2	Flat plate lower surface	Backing plate upper surface		
3	Equipment cabin bracket lower surface	Flat plate upper surface		

bottom cover assembly and manufacturability, six parameters are selected as shown in Figure 9.

Among them, d is the distance between the rivet hole and the plate end, d_1 is the lateral hole distance of the rivet hole, p is the longitudinal spacing of the rectangular tube beam, w is the width of the rectangular tube beam midsurface, h is the height of the rectangular tube beam midsurface, and t is the thickness of the rectangular tube beam. The parameters d and d_1 are related to the lateral number of rivets b:

$$d_1 = \frac{(d_c - 2\ d)}{b}, \tag{15}$$

where d_c is the lateral length of the flat plate, and the original values and value ranges of each parameter are shown in Table 4.

Using the SA method described in Section 2.2, the stress-influence sensitivity of each parameter under the two working conditions of pull and push at 4 kPa aerodynamic loads is shown in Figure 10.

It can be seen from Figure 10that the sensitivity of the parameters$h$, t, and$w$is high, indicating that their changes have the most significant impact on the stress. These three parameters are selected as the optimization parameters, and the other parameters have less impact and are ignored in the optimization.

4.2. Parameter Sampling and Calculation. Based on the selected parameters, the range of values is the same as that shown in Table 3, and the optimal Latin hypercube method is

Table 2: Comparison of FE simulation and test results of some measuring points.

Measurement point	Pull 4 kPa uniform load		Push 4 kPa uniform load	
	Measured stress/MPa	Simulation stress/MPa	Measured stress/MPa	Simulation stress/MPa
2	−10.4	−9.0	5.7	6.6
3	−14.9	−12.7	12.3	12.2
4	−7.6	−9.0	6.0	6.7
12	−31.8	−37.1	22.4	26.1
13	−55.7	−64.3	40.4	48.9
14	−36.8	−36.8	24.6	27.3
15	−36.0	−36.2	24.0	27.7
16	−58.1	−65.2	41.5	48.0
17	−37.9	−36.7	23.7	27.6

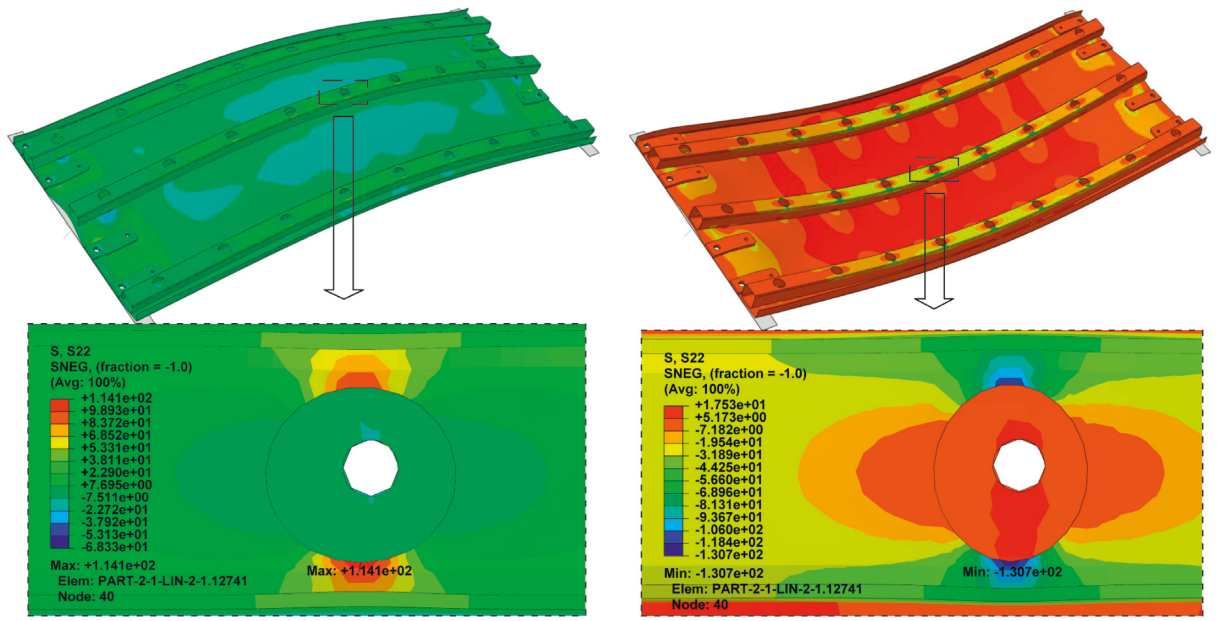

(a) (b)

Figure 8: Stress distribution on the edge of the center process hole rectangular tube beam. (a) Push working condition. (b) Pull working condition.

Table 3: Mechanical properties of SUS304 cold-rolled stainless steel plate.

Material	Yield strength σ_b/MPa	Ultimate strength σ_u/MPa
SUS304	320	660

used to sample them. In order to meet the fitting needs of the surrogate model, the sampled data are initially set to 50 groups. The distribution in the parameter space is shown in Figure 11.

It can be seen from Figure 11 that the distribution of each sample in the parameter space is relatively uniform and representative. Use the Python program to input these 50 groups of samples into ABAQUS to establish a parameter model, complete the preprocessing of the model, and run it in batches. Read the maximum normal stress of the process hole edge of the square tube beam under two different working conditions of the flat plate under push and pull of 4 kPa aerodynamic load and calculate the equivalent stress as the output parameter in combination with (14). The 50 groups of input and output parameters after all simulations are completed and are shown in Table 5.

The 50 sets of input and output parameters in Table 5 can be used as training samples for the surrogate model and input into Isight for approximate fitting.

4.3. Surrogate Model Fitting. Use different fitting models to fit the training samples in Table 5. Based on the cross-validation method, two indexes of NRMS and R2 are used to evaluate the goodness of fit. The goodness of fit indexes under different models are obtained as shown in Table 6.

From Table 6, the indexes of the RBFNN model are all the best, so the RBFNN model is used as the surrogate model of the original model. The comparison between the predicted value of the output and the original value is shown in Figure 12.

It can be seen from Figure 12that the distribution of the predicted value and the original value points are all around

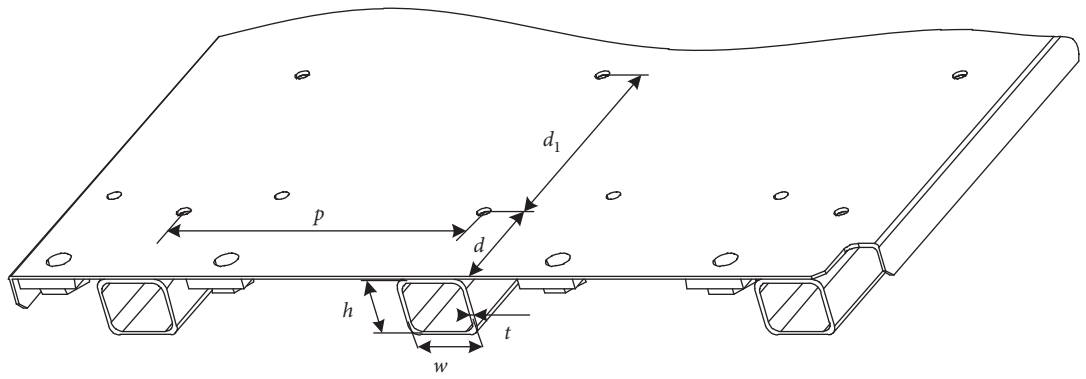

Figure 9: Parameter determination.

Table 4: The original value of each parameter and its range.

No.	Parameter	Original values	Lower limit	Upper limit
1	d	60 mm	30 mm	100 mm
2	p	193 mm	168 mm	243 mm
3	w	35 mm	35 mm	50 mm
4	h	28 mm	12 mm	50 mm
5	t	2 mm	1 mm	3 mm
6	b	9	7	11

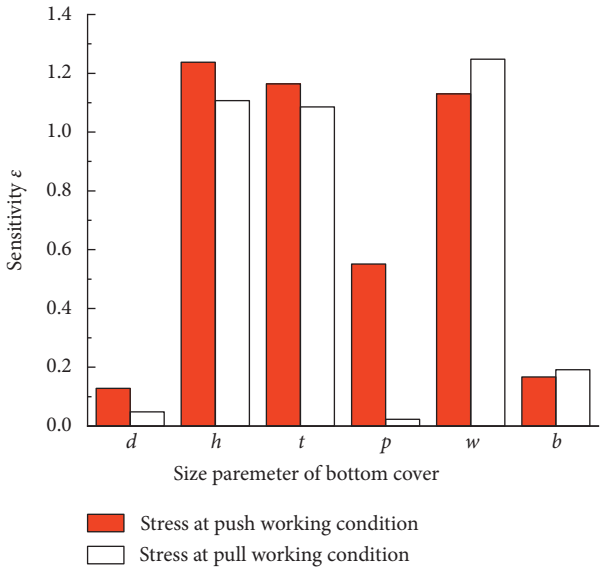

Figure 10: Sensitivity index of different parameters.

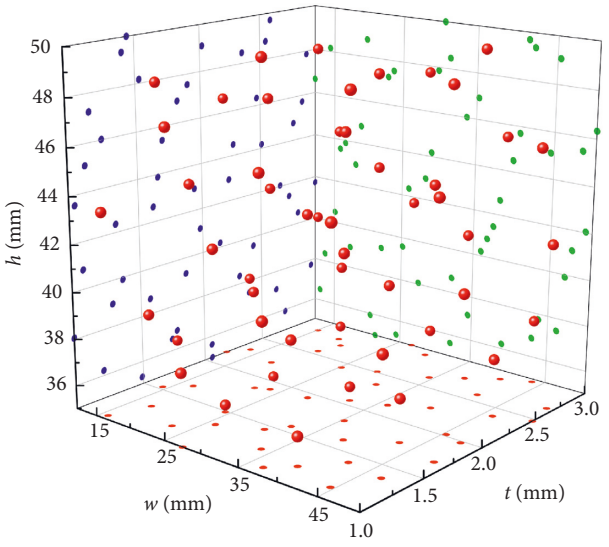

Figure 11: Parameter sample space.

the straight line $y = x$, indicating that the fitting accuracy is high. The fitted surrogate model can be used as a simplified model to replace the original model for optimization.

4.4. Parameter Optimization Solution and Verification. Based on the above surrogate model, it can be optimized and solved in Isight. The optimized value range of each parameter is shown in Table 4. Determine the optimization goal to minimize the equivalent stress:

$$\min\{\sigma_{-1}\}. \tag{16}$$

In order to control the weight of the optimized bottom cover, corresponding constraint conditions need to be set. Since the above parameters only relate to the cross-sectional area of the rectangular tube beam, the weight of the bottom cover can be controlled by controlling the optimized cross-sectional area of the rectangular tube beam. In the original structure, the square tube beam midsurface height $h = 28$ mm, midsurface width $w = 35$ mm, and thickness $t = 2$ mm; ignoring rounded corners, its area is $S = (35 + 28) \times 2 \times 2 = 252\ \text{mm}^2$. Therefore, the optimization constraints can be expressed as

$$s.t.\ S = 2t(w + h) \le 252. \tag{17}$$

Table 5: Surrogate model training samples.

No.	w/mm	h/mm	t/mm	Equivalent stress/MPa
1	19.76	2.55	48.78	78.0
2	36.04	2.14	40.20	67.2
3	32.16	1.57	38.67	115.6
4	46.90	1.37	39.90	85.9
5	36.82	1.08	40.82	129.0
6	38.37	1.61	42.65	73.9
7	12.78	1.74	36.53	218.2
8	23.63	1.90	47.55	95.8
9	50.00	2.47	46.33	31.3
10	12.00	2.18	46.63	127.8
11	43.80	2.96	37.76	37.4
12	34.49	2.63	37.14	59.9
13	25.18	2.43	39.59	82.4
14	28.29	1.94	42.96	86.5
15	35.27	1.82	46.94	65.8
16	29.06	2.51	44.18	62.2
17	15.10	2.84	40.51	113.2
18	17.43	1.29	38.98	211.3
19	31.39	2.35	48.47	54.1
20	15.88	1.04	43.57	241.2
21	30.61	1.45	50.00	88.7
22	24.41	1.49	35.31	191.9
23	20.53	2.71	35.92	116.2
24	27.51	1.00	38.06	199.8
25	42.24	1.41	49.39	78.0
26	44.57	1.12	45.10	84.9
27	18.20	2.22	42.96	110.1
28	45.35	2.02	49.08	113.2
29	18.98	2.80	44.80	44.9
30	25.96	1.33	42.35	79.3
31	41.47	2.59	49.69	142.5
32	22.86	1.16	47.24	162.8
33	13.55	2.31	38.37	33.2
34	33.71	1.25	46.02	151.5
35	16.65	1.65	43.88	104.0
36	26.73	3.00	41.73	150.8
37	39.92	2.27	44.49	61.3
38	39.14	1.20	36.22	46.4
39	47.67	1.98	41.12	124.5
40	43.02	1.78	36.84	48.1
41	14.33	1.53	48.16	69.8
42	21.31	2.06	35.00	160.3
43	49.22	2.67	42.04	161.0
44	40.69	2.88	45.71	31.8
45	32.16	2.06	35.61	35.5
46	22.08	1.86	39.29	97.5
47	37.59	2.76	41.43	121.4
48	48.45	1.69	45.41	45.3
49	46.12	2.39	37.45	56.2
50	29.84	2.92	47.86	44.5

Using the original parameters as the initial values, after calculation, the iteration times and optimization results of the NLPQLP and MIGA optimization algorithms are obtained as shown in Table 7. It can be seen that the convergence results of the two optimization methods are similar, so the optimization calculation results are credible. Among them, the numerical optimization method is less time-consuming than the exploratory optimization method. The optimization history of the equivalent stress under the two algorithms is shown in Figure 13 where the red point is the point that does not meet the constraint, the black point is the general point, and the green point is the optimal point.

From the above optimization process, it can be seen that the search speed of the NLPQLP algorithm is faster, but the number of iterations has reached 74. The optimization speed of the MIGA method is slower, but it can perform a global search in the parameter space.

Table 6: Goodness of fit under different fitting algorithms.

Fitting model	Goodness of fit	
	NRMS	R^2
Second-order RSM model	0.033	0.982
Third-order RSM model	0.032	0.984
Fourth-order RSM model	0.032	0.984
RBFNN model	0.028	0.988
Kriging model	0.080	0.900
Chebyshev polynomial model	0.032	0.984

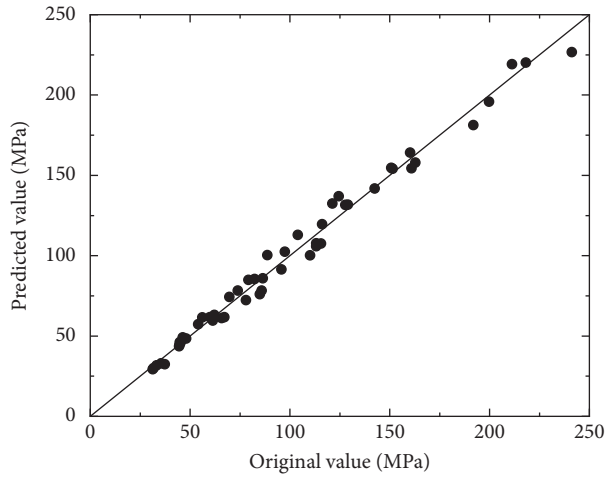

Figure 12: Comparison between predicted value and original value.

Table 7: Optimization results under different optimization algorithms.

Optimization algorithms	Iteration times	Optimization result		
		w/mm	h/mm	t/mm
NLPQLP	74	43.333	39.151	1.5276
MIGA sub-population size: 40; number of generations: 50; number of islands: 10	20001	44.342	39.308	1.5063

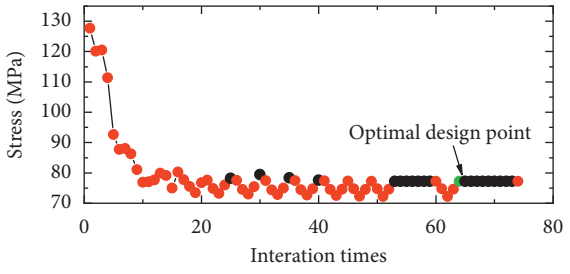

(a)

Figure 13: Continued.

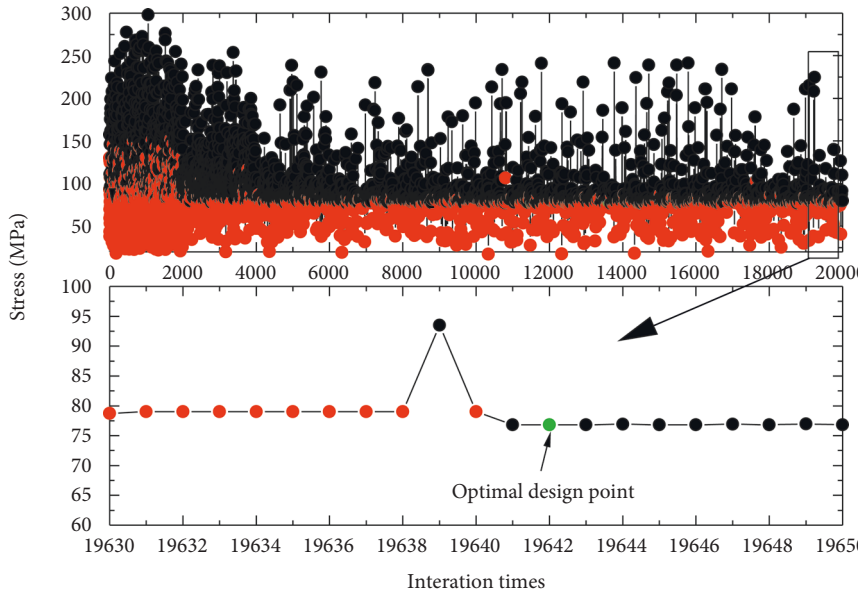

Figure 13: Optimization iteration process. (a) NLPQLP. (b) MIGA.

Table 8: Comparison between the optimized model and the original model.

	w/mm	h/mm	t/mm	S/mm2	σ_{-1}/MPa
Original model	35.0	28.0	2.0	252.0	126.7
Optimized model	44.0	39.0	1.5	249.0	78.9
Optimization rate				1.2%	37.7%

Based on the optimization results in Table 7, round the parameters and input them into ABAQUS for FE simulation verification. The output and the original model are shown in Table 8.

It is shown in Table 8 that the equivalent stress of the hole edge of the optimized model is significantly optimized compared with the original model, the optimization rate reaches 37.7%, and its weight is also reduced. The optimization effect is significant.

5. Summary

(1) Establish the parameterized model of the bottom cover by ABAQUS + Python jointly development method. Obtain the output samples in batches according to the input samples, which eliminates tedious pre and postprocessing and can improve the efficiency of sample acquisition.

(2) Comparing the FE model with the bench test results of the equipment cabin bottom cover, the stress levels at each measurement point are basically the same, indicating that the boundary conditions and contact conditions of the FE model can basically simulate the actual model. Its accuracy can ensure the subsequent optimization design.

(3) The bottom cover is optimized based on the SA method and surrogate model. After optimization, the equivalent stress at the edge of the model hole decreased from 126.7 MPa to 78.9 MPa, which was optimized by 37.7%. The optimization effect was significant.

(4) This study only needs to perform 50 simulations on the FE model to obtain samples, and the surrogate model method can save thousands of repeated optimization calculations on the FE model. Therefore, based on the method in this paper, the optimization efficiency can be improved for complex FE models.

Data Availability

The data used to support the findings of this study are available from the corresponding author upon request.

Conflicts of Interest

The authors declare that they have no conflicts of interest.

Acknowledgments

This study was supported by the National Natural Science Foundation of China (11790281).

References

[1] A. Vazdirvanidis, S. Papadopoulou, S. Papaefthymiou, G. Pantazopoulos, and D Skarmoutsos, "Failure investigation of Cu-DHP tubes due to ant-nest corrosion," *International Journal of Structural Integrity*, vol. 10, no. 3, pp. 325–336, 2019.

[2] M. D. Nor, S. N. Mat Saliah, and A. Ibrahim, "Fatigue damage severity assessment of RC beam[J]," *International Journal of Structural Integrity*, vol. 10, no. 5, pp. 612–620, 2019.

[3] R. Manouchehry Nya, S. Abdullah, S. Singh Karam Singh, and S. Singh, "Reliability-based fatigue life of vehicle spring under random loading," *International Journal of Structural Integrity*, vol. 10, no. 5, pp. 737–748, 2019.

[4] W. Zhou, L. Chen, Z. Wang, S. Ding, and Y. Shan, "Aerodynamic load spectrum and fatigue behaviour of high-speed train's equipment cabin," *Fatigue and Fracture of Engineering Materials and Structures*, vol. 42, no. 11, pp. 2579–2595, 2019.

[5] D. Meng, S. Yang, C. He et al., "Multidisciplinary design optimization of engineering systems under uncertainty: a review," *International Journal of Structural Integrity*, vol. 13, no. 4, pp. 565–593, 2022.

[6] C. Yang and Q. M. Li, "Structural optimisation for the collapse zone of a railway vehicle," *International Journal of Mechanical Sciences*, vol. 165, 2020.

[7] H. A. Lee, S. B. Jung, H. H. Jang et al., "Structural-optimization-based design process for the body of a railway vehicle made from extruded aluminum panels," *Proceedings of the Institution of Mechanical Engineers-Part F: Journal of Rail and Rapid Transit*, vol. 230, no. 4, pp. 1283–1296, 2016.

[8] T. Kuczek, "Application of manufacturing constraints to structural optimization of thin-walled structures," *Engineering Optimization*, vol. 48, no. 2, pp. 351–360, 2016.

[9] Q. Xiao, W. Guo, L. Yang, S. Zhou, and D. Chen, "Design and topology optimization of air conditioning suspension bracket for metro," *Science Progress*, vol. 103, no. 4, 22 pages, Article ID 003685042098061, 2020.

[10] D. Wennberg and S. Stichel, "Multi-functional design of a composite high-speed train body structure," *Structural and Multidisciplinary Optimization*, vol. 50, no. 3, pp. 475–488, 2014.

[11] D. Lang and D. W. Radford, "Design optimization of a composite rail vehicle anchor bracket," *Urban Rail Transit*, vol. 7, no. 2, pp. 84–100, 2021.

[12] H. S. Kim, C. W. Ahn, and K. H. Choi, "Shape optimization of a bogie frame for the reduction of its weight[J]," *Journal of the Korean Society for Precision Engineering*, vol. 19, no. 9, pp. 186–192, 2002.

[13] M. Yamamoto, "Non-parametric optimization of railway wheel web shape based on fatigue design criteria," *International Journal of Fatigue*, vol. 134, Article ID 105463, 2020.

[14] C. Y. Hou, Y. F. Lee, and Y. H. Peng, "Fatigue damage analysis of steel components subjected to earthquake loadings," *International Journal of Structural Integrity*, vol. 10, no. 1, pp. 25–40, 2019.

[15] A. Takale and N. Chougule, "Optimization of process parameters of wire electro discharge machining for $Ti_{49.4}Ni_{50.6}$ shape memory alloys using the Taguchi technique," *International Journal of Structural Integrity*, vol. 10, no. 4, pp. 548–568, 2019.

[16] A. H. Makwana and A. A. Shaikh, "Towards hybridization of composite patch in repair of cracked Aluminum panel," *International Journal of Structural Integrity*, vol. 10, no. 6, pp. 868–887, 2019.

[17] D. Meng, S. Yang, T. Lin, J. Wang, H. Yang, and Z. Lv, "RBMDO using Gaussian mixture model-based second-order mean-value saddlepoint Approximation," *Computer Modeling in Engineering and Sciences*, vol. 132, no. 2, pp. 553–568, 2022.

[18] M. Mrzyglod and A. P. Zielinski, "Parametric structural optimization with respect to the multiaxial high-cycle fatigue criterion," *Structural and Multidisciplinary Optimization*, vol. 33, no. 2, pp. 161–171, 2006.

[19] M. Mrzyglod and A. P. Zielinski, "Multiaxial high-cycle fatigue constraints in structural optimization," *International Journal of Fatigue*, vol. 29, no. 9-11, pp. 1920–1926, 2007.

[20] W. Sun, J. Zhou, D. Gong, and T. You, "Analysis of modal frequency optimization of railway vehicle car body," *Advances in Mechanical Engineering*, vol. 8, no. 4, 12 pages, Article ID 168781401664364, 2016.

[21] C. W. Hudson, J. J. Carruthers, and A. M. Robinson, "Multiple objective optimisation of composite sandwich structures for rail vehicle floor panels," *Composite Structures*, vol. 92, no. 9, pp. 2077–2082, 2010.

[22] B. R. Miao, Y. X. Luo, Y. J. Qiu, Q. Peng, C. Jiang, and Z. Yang, "Research on multidisciplinary fatigue optimization design method in structural design of high speed train," *Procedia Structural Integrity*, vol. 22, pp. 102–109, 2019.

[23] B. Miao, W. Zhang, J. Zhang, and D. Jin, "Evaluation of railway vehicle car body fatigue life and durability using a multi-disciplinary analysis method," *International Journal of Vehicle Structures & Systems*, vol. 1, no. 4, p. 85, 2009.

[24] P. Zhi, Y. Li, B. Chen, M. Li, and G. Liu, "Fuzzy optimization design-based multi-level response surface of bogie frame," *International Journal of Structural Integrity*, vol. 10, no. 2, pp. 134–148, 2019.

[25] S. Baek, X. Song, and M. Kim, "Multiobjective optimization of beam structure for bogie frame considering fatigue-life extension[J]," *Journal of Electrical Engineering & Technology*, pp. 1–11, 2021.

[26] H. Zhang, Y. Peng, L. Hou, G. Tian, and Z. Li, "A hybrid multi-objective optimization approach for energy-absorbing structures in train collisions," *Information Sciences*, vol. 481, pp. 491–506, 2019.

[27] J. Chen, P. Xu, and S. Yao, "The multi-objective structural optimisation design to improve the crashworthiness of a multi-cell structure for high-speed train[J]," *International Journal of Crashworthiness*, pp. 1–10, 2020.

[28] J. Li, G. Gao, and H. Dong, "Crushing analysis and multi-objective optimization of a railway vehicle driver's cab," *Thin-Walled Structures*, vol. 107, pp. 554–563, 2016.

[29] B. Park, N. Kim, and J. Kim, "Optimum design of tilting bogie frame in consideration of fatigue strength and weight[J]," *Vehicle System Dynamics*, vol. 44, no. 12, pp. 887–901, 2006.

[30] Y. Gao and W. Zhao, "Adaptive optimization with weld fatigue constraints based on surrogate model for railway vehicles," *Mechanics Based Design of Structures and Machines*, vol. 42, no. 2, pp. 244–254, 2014.

[31] Y. Gao, Q. Liu, and D. Zhao, "Kriging surrogate model based optimisation of welded bogie frame for fatigue improvement [J]," *International Journal of Vehicle Structures & Systems*, vol. 11, no. 4, pp. 349–354, 2019.

[32] Z. Xia, J. Liu, and Y. Cheng, "Fast prediction of mechanical impedance of an underwater foundation based on surrogate models[J]," *Chinese Journal of Ship Research*, vol. 15, no. 03, pp. 81–87, 2020.

[33] H. Zou, S. Sun, and L. I. Qiang, "Device for Applying Surface Load: China: CN104677651A[P]," 2015.